Draft version May 13, 2019
Typeset using LaTeX **twocolumn** style in AASTeX62

Non-grey month-long brightening of KIC 8462852 in the immediate aftermath of a deep dip

James Hitchcock,[1,*] Stephen J. Fossey,[1,2] and Giorgio Savini[1,2]

[1] *Department of Physics and Astronomy, University College London, Gower Street, London, WC1E 6BT, United Kingdom*
[2] *University College London Observatory, 553 Watford Way, London, NW7 2QS, United Kingdom*

(Received May 13, 2019; Revised May 13, 2019; Accepted XXX)

Submitted to PASP

ABSTRACT

We present an analysis of the results of long-term multi-band photometric monitoring of the enigmatic star, KIC 8462852. Observations in the B, g', V, r' and I_C passbands have been acquired at University College London Observatory (UCLO) between May 2017 and September 2018. We interrogate the wavelength dependence of the ∼month-long dimming and brightening exhibited by the target star over an 85-day interval, immediately following a days-long ∼ 5 per cent drop in brightness on Julian Date (JD) 2458203. Between JD 2458215–300 we measure brightness variations which correspond to relative extinctions of $A_B/A_V = 1.39 \pm 0.27$, $A_{g'}/A_V = 1.16 \pm 0.11$, $A_{r'}/A_V = 0.80 \pm 0.25$ and $A_{Ic}/A_V = 0.49 \pm 0.19$, from which we infer an Ångström absorption coefficient of 1.33 ± 0.43 ($R_V \simeq 3.2^{+2.6}_{-1.0}$). As with the days-long 'dips', the wavelength dependence of the longer-term brightness variations must also be associated with extinction arising from a dust distribution containing a substantial fraction of sub-micron-sized grains. This implies some common causal phenomenon to be responsible for the star's brightness fluctuations, which is not dependent on the timescale of variation. This implies some common mechanism is responsible for the star's variability on timescales of the order of both days, months, years and even centuries.

Keywords: stars: individual (KIC 8462852) – stars: peculiar – dust, extinction

1. INTRODUCTION

Since its discovery by citizen scientists in *Kepler* data, KIC 8462852 has gained a reputation as one of the most unusual stars in the Galaxy.In their discovery paper, Boyajian et al. (2016) describe this F-type main sequence star's unprecedented behavior, in which it was shown to undergo 'dips' in its flux over day-long timescales of up to 22 per cent. Through follow-up ground-based multi-band photometric monitoring, it is now known that the dips have a wavelength dependence associated with extinction from astrophysical dust with a substantial fraction of submicron sized particles ($< 0.3\mu m$ in diameter) (e.g. Boyajian et al. 2018; Deeg et al. 2018).

Corresponding author: James Hitchcock
james.hitchcock.17@ucl.ac.uk

* The author is currently affiliated with the University of St. Andrews.

A study of archival photographic plates by Schaefer (2016) found that KIC 8462852 has faded in the B-band at an average rate of 0.164 ± 0.013 magnitudes per century between 1890 and 1989. Variations in flux over year-long timescales have been measured by both Meng et al. (2017) and Davenport et al. (2018), who measured a fairly neutral extinction of $R_v \geqslant 5$ and $R_V = 5.0 \pm 0.9$ respectively. More recently, Schaefer et al. (2018) have shown that colour-dependent variations in flux of a few per cent occur on month-long timescales. From a total of 1866 $BVRI$ nightly magnitudes binned over 20-day intervals, an extinction law steeper than $R_V \sim 5$ is inferred, and is found to be consistent with that of canonical ISM extinction ($R_v = 3.1$), again suggestive of sub-micron-sized grains. This is an average value to describe the entire 2.43-year-long $BVRI$ light curve, and suggests that the material responsible for both the dips and longer-term dimming have a common origin.

Bodman et al. (2018) note that no single wavelength dependence describes the series of dipping events of

May–September 2017. The authors claim there is a tentative detection of non-grey long-term dimming on which the dips are superimposed. It is suggested that the chromaticism associated with this longer-term variation becomes increasingly neutral as the dip complex progresses, and the extinction is markedly steeper during the first dip (*Elsie*) than the fourth and final dip (*Angkor*) four months later.

In March and April of 2018, ground-based photometric observations of the ongoing Las Cumbres Observatory monitoring campaign revealed KIC 8462852 to undergo two further dips (labelled *Caral Supe* and *Evangeline*) of ~ 5 per cent, the deepest seen since the *Kepler* mission [1]. Since May 2017, we have been carrying out multi-band photometric monitoring of KIC 8462852 using observations from the University College London Observatory (UCLO). In particular, our coverage of $BVg'r'I_c$ photometry in the 85 days following the *Caral Supe* and *Evangeline* dips allows an investigation into the nature of the material assumed to be trailing the object(s) associated with these dips. The paper is laid out as follows: in Section 2 we report our observations and photometric calibrations to transform our photometry to the BVI_C and $g'r'$ standard systems; section 3 presents our results, in which we demonstrate the chromatic dependence of the extinction over this 85-day interval, and obtain a value for the Ångström absorption coefficient, α, and the ratio of total-to-selective extinction, R_V, for the inferred population of dust grains. Section 4 discusses our conclusions.

2. METHODS

2.1. *UCLO observations*

Observations of KIC 8462852 at UCLO span from May 2017 to September 2018. Two Celestron C14 (0.35-m) robotic telescopes were used for this observing campaign, and observations were made through a total of eight filters: 'Green' (as a proxy for V) and Astrodon R_CI_C filters on the C14 West telescope (with SBIG STL6303E CCD), and Astrodon $BVg'r'i'$ filters on the C14 East (with FLI PL9000 CCD), amounting to more than 400 mean magnitudes across all filters. Typically, ten images were obtained in each filter on each night, with exposure times ranging from 50–75 seconds per image. All images were processed with standard bias, dark, and flat-field reductions each night.

2.2. *Photometry*

Our approach to obtaining adequate precision in the long-term photometry is outlined below.

[1] https://www.wherestheflux.com/blog/page/4

Photometric measurements of KIC 8462852 and reference field stars were made using the Source Extractor (SExtractor) software Bertin & Arnouts (1996), with automated Kron apertures being preferred; we have found that the use of Kron apertures in our images yields marginally better statistics than fixed-radius circular apertures, probably due to a non-circular aperture adapting to variations in the stellar point-spread-function across the field.

Our observing strategy ensured that for each telescope series, the target and reference stars were located in the same position on the chip each night, within the precision of the 'plate-solve-and-guide' robotic time-series.

We ensured that we had sufficient total integrated flux to obtain the required statistical precision within a single night's observations: typical integrated fluxes of 1–2×10^5 photoelectrons were obtained in KIC 8462852, per image, yielding $> 10^6$ photoelectrons per night in each filter.

Variations in the flux of KIC 8462852 are of the order of at least 1 per cent for both the short-timescale dips and longer-timescale dimming and brightening. As such, the required precision of the photometry to establish statistically significant variations in the target is at the millimagnitude (mmag) level. The intrinsic photometric uncertainty was typically 4–5 mmag for a single frame, dominated by Poisson noise on the star signal and scintillation noise (given the relatively short exposure times). We averaged the magnitudes derived from multiple (typically, ten) images in a single night, but clipped to exclude $> 5\sigma$ outliers — avoiding the effects of, e.g., bad/hot pixels, cosmic rays — such that the statistical uncertainty can be reduced to achieve an internal precision of 1–2 mmag per night for bright sources central to the CCD.

We evaluate the effect of systematic errors which can arise in ground-based photometry (e.g., see Schaefer et al. (2018)) by examining the long-term stability of the reference-star magnitudes in our own data — both to select stable, non-variable comparison stars for the photometric calibration; and also as a check on the final residual photometric uncertainties from night to night (§2.4).

2.3. *Transformation to standard passbands and reference star selection*

Photometric calibration of KIC 8462852 was achieved with reference to bright, unsaturated, nearby standard stars in the field for which standard magnitudes were available in the APASS catalogue (Henden et al. 2016). Lahey et al. (2017) measure a superior photometric precision in the V and I_C bands for many of the reference

stars used in the calibration, and where available, we preferred these measurements over the APASS values.

In order to correct for the wavelength-dependent mismatch between our instrument system and the standard passbands, and time-variable effects of atmospheric extinction, transformation of our instrument magnitudes at a given airmass, X, $m_{\rm inst}(X)$, into the appropriate standard-system passband, $m_{\rm std}$ (as provided by either APASS or Lahey et al. (2017)), was achieved through the equation

$$m_{\rm inst}(X) - m_{\rm std} = z + \epsilon C_{\rm std}, \quad (1)$$

where $C_{\rm std}$ is a star colour in standard passbands, such as $(B-V)$, and z and ϵ are the transformation coefficients derived from a weighted fit to standard-star magnitudes and colours (as in the example shown in Fig. 1). The standard star colours used in equation 1 depend on the bandpass transformation: for B, V, and g', APASS $(B-V)$ colours (Henden et al. (2016)) were used; for r' and I_c, $(r'-I_c)$ colours derived from the APASS and Lahey et al. (2017) values were used.

The reference stars used in the calibrations for all filters are the most stable stars from an initial sample of 20 candidate reference stars; we derived a standard magnitude for each reference star, and examined their stability over the entire observing campaign — for each filter, the stars which had a standard deviation exceeding 10 mmag were iteratively removed, and the calibration was re-performed with the improved sample, until all calibration stars were found to be stable at better than 10 mmag precision over the entirety of the observing campaign, and across all passbands presented in this work. The standard deviation of their ∼1.3-year-long time series is typically better than 5 mmag; for bright sources, central on the CCD, their standard deviation was as low as 1–2 mmag in all passbands, and the level of the within-night variation measured for these stars can be < 1 mmag. Finally then, up to eight, and no less than five, reference stars were ultimately used for the transformations, dependent on the filter (see Table 1).

The final uncertainty used to weight each reference star in the fits to equation 1, in each filter, was calculated from the orthogonal sum of its standard deviation in the campaign time series and the standard error on its mean magnitude within each night's data.

Substitution of these values in place of the 'external' uncertainties provided in the APASS catalogue was also motivated by inspection of the reduced chi-squared values in the fits to equation 1, which were much closer to unity.

Finally, from the transformation coefficients derived for each image, the instrument magnitudes for KIC 8462852 were transformed to standard magnitudes using equation 1, for each passband indicated in Table 1. The standard colours used for KIC 8462852 were $(B-V) = 0.508$ (Henden et al. (2016)) and $(r'-I_C) = 0.487$ (based on Henden et al. (2016) and Lahey et al. (2017) (we always used at least one reference star with a colour at least as blue as that of KIC 8462852 to help establish a reliable colour term in equation 1).

Telescope/Filter[a]	Exp. time (seconds)	Standard System [b]	N(ref)[c]
C14 West / Green	60	V	7
R_C	50	r'	8
I_C	75	I_C	8
C14 East / B	75	B	6
g'	50	g'	6
V	50	V	6
r'	50	r'	5
i'	75	I_C	5

Table 1. Observational and calibration information for all telescopes/filters used here. (*a*) The telescope/filters used in this observing campaign; (*b*) the standard photometric systems to which the measured instrument magnitudes in each filter are transformed (equation 1); (*c*) the number of reference stars used for the transformation.

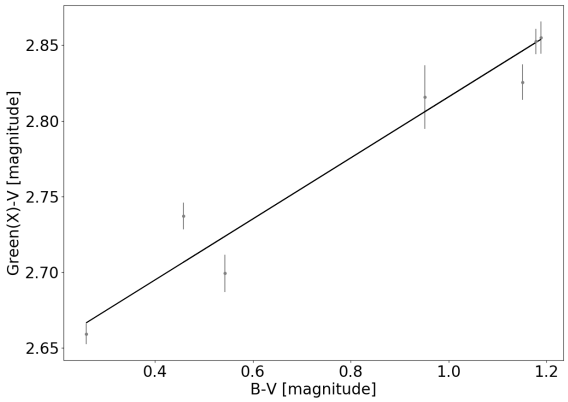

Figure 1. A typical scatter plot from the derivation of the transformation coefficients (i.e, the intercept, z, and slope, ϵ, in equation 1). This particular plot illustrates the calibration of an instrument magnitude in the C14 West *Green* filter (denoted as a function of airmass, X) transformed to the standard V passband.

2.4. *Night-to-night uncertainties for KIC 8462852*

As noted in §2.2, we can determine intrinsic 'within night' uncertainties for the magnitude of KIC 8462852.

To account realistically for potential systematic variability from night to night (and hence guard against over-interpretation of brightness variations), we attempt to quantify a systematic uncertainty on each night associated with its transformed standard magnitude. This may be derived from the nightly scatter of the reference-star magnitudes: for any given night, one can calculate the median absolute deviation (MAD) of the reference-star magnitudes, in each filter, relative to their median brightness in the campaign time series, to derive an uncertainty per filter, per night. For night i, and reference star j,

$$\sigma_i = 1.4826 \times \text{median}(|m_{ij} - m_{j,\text{median}}|). \quad (2)$$

Equation 2 hence describes a residual systematic uncertainty, σ_i, in the standard star magnitudes, for each filter per night, which is combined quadratically with the standard error on the mean of the KIC 8462852 standard magnitudes obtained on the same night. These total per-night uncertainties for KIC 8462852 are those shown in Figures 2, and were used in the weighting of the fits illustrated in Figure 3.

2.5. *Combining C14 West and C14 East magnitudes*

Systematic differences may also occur between observations of the target acquired in different filters on different telescopes, for which we have used different comparison stars. In order concurrently to analyse filter datasets that have been transformed to the same standard photometric bandpass, we renormalise one set of telescope magnitudes to another, separately for V, r', and I_C (Table 1). This is done by evaluation of the function:

$$f = \sum_i^{N_a} \sum_j^{N_b} \frac{(y_{a,i} - (y_{b,j} + \Delta m))^2}{\sigma_{a,i}^2 + \sigma_{b,j}^2} \times \exp\left[-\frac{(t_{a,i} - t_{b,j})^2}{2l^2} \right], \quad (3)$$

(after Osborn et al. (2019)), where t_a, t_b and y_a, y_b represent times (JD) and magnitudes for series a and b, comprising N_a and N_b data points, with magnitude uncertainties σ_a and σ_b. The constant l is fixed to represent the typical shortest-timescale variation of KIC 8462852, and is set here to be 1 day. The magnitude offset Δm is optimised for a given filter, by minimising the function f. In this way, a single dataset containing both C14 East and renormalised C14 West observations may be used in the analysis. We chose to renormalise C14 West measurements to the C14 East measurements for all relevant filter datasets, owing to the latter's greater coverage when both telescopes were operational in the campaign (i.e., the observing window which follows the May 2017 dip events, see Figure 2).

3. RESULTS AND DISCUSSION

The UCLO light curve from May 2017 to September 2018 for all passbands used in this work is shown in Fig. 2. [2] As in the Schaefer et al. (2018) light curve — which spans the the JD window 2457300–8200 — the amplitude of variation in B can be seen to exceed that in all other bands. Unfortunately, a gap in UCLO coverage means we missed the *Caral-Supe* dip and the minimum of the *Evangeline* dip. However, we do capture the egress of the *Evangeline* dip; over the 85-day window immediately following *Evangeline*, KIC 8462852 undergoes a net brightening, interspersed with shorter-timescale variation, shown as the shaded region in Fig. 2. In the following, we interrogate the wavelength dependence associated with this 85-day interval.

3.1. *Measurements of extinction in the Julian date window 2458215-300*

For each mean magnitude in the combined C14 East and West V-band data sets, the closest temporal measurement in the other passbands is found. Provided these measurements were acquired within 0.1 days of each other, the data are considered to be concurrent and matched. On nights where both the C14 West and C14 East were observing, a single nightly average magnitude in passband X (where $X = B$, g', r', or I_C) may be matched against both the V-band measurements obtained by both telescopes. To avoid 'doubling-up' of data, only the closest temporal match is kept.

A measure of the relative extinction between the different passbands, assumed responsible for these variations, can be determined from a linear fit to the magnitudes obtained in one passband relative to another. Fig. 3 shows weighted linear fits to the nightly average magnitudes in B, g', r' and I_C passbands against the V-band magnitude for the JD window 2458215–300.

In order to account for the intrinsic scatter and the heteroscedastic measurement errors on both axes in the regression plots (i.e., the size of the errors is dependent on systematic effects that vary from one observation to the next), a BCES (bivariate correlated errors and intrinsic scatter) fitting routine was employed (Akritas & Bershady (1996)); an orthogonal least-squares fit is used. The measured slopes, which are equivalent to the ratios of the relative extinctions, A_λ/A_V, and shown in Fig. 3, are given in Table 2; we adopt the convention of a normalised measurement of extinction relative to the V-band, A_λ/A_V (where $\lambda = B$, g', r', or I_C). The

[2] Note that for purposes of display, all magnitudes have been offset relative to the V-band. A full table of the non-offset magnitudes and their associated errors is provided in Appendix A.

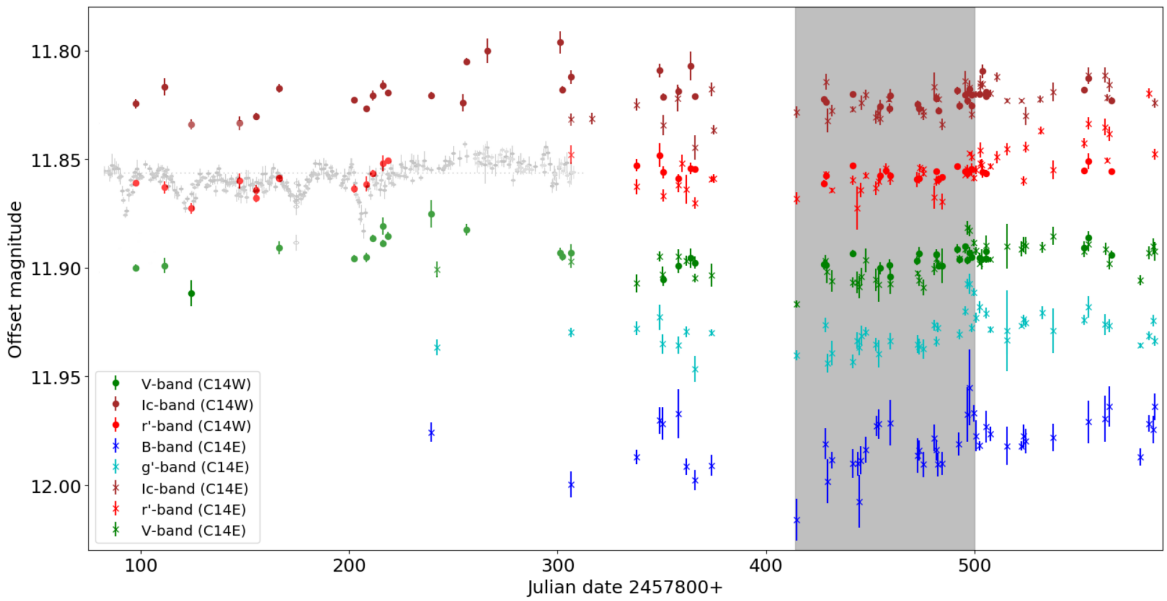

Figure 2. The 1.3-year-long UCLO $BVg'r'I_c$ light curves for the target star, KIC 8462852. The magnitude time series is characterized by wavelength-dependent dimming and brightening of variable timescales. The gray shaded region describes the Julian date (JD) window (2457800+) 415-500, i.e., the interval analyzed in this study. The May–September 2017 dip events cover the 80–220 interval, over which we superimpose the r'-band light curve from Figure 2 of Boyajian et al. (2018). The *Caral-Supe* and *Evangeline* dips occur in the interval 390-430. All magnitudes are offset relative to the V-band to aid comparison (see Appendix A), and the error bars shown are the orthogonal sum of the standard error on the nightly averages and the σ_i statistic described in 2.4. We denote data taken on the C14 West (C14W) and East (C14E) with filled circles and crosses respectively.

relative extinctions were then used to fit the function,

$$\tau_\lambda/\tau_{\lambda_V} = (\lambda/\lambda_V)^{-\alpha}, \quad (4)$$

where the optical-depth ratios, $\tau_\lambda/\tau_{\lambda_V}$ can be assumed to be equal to the slopes A_λ/A_V if $A_\lambda << 1$, λ is the effective passband wavelength, and α is the absorption Ångström coefficient (Moosmüller et al. (2011), Deeg et al. (2018)). From a weighted least-squares fit to the data we infer $\alpha = 1.33 \pm 0.43$. This best fit result is corroborated by a Monte Carlo resampling and refitting of the Table 2 values, with comparable, and normally distributed (i.e., symmetric) uncertainties.

Extinction ratio	Slope and uncertainty
A_B/A_V	1.39 ± 0.27
$A_{g'}/A_V$	1.16 ± 0.11
$A_{r'}/A_V$	0.80 ± 0.25
A_{Ic}/A_V	0.49 ± 0.19

Table 2. The slopes from orthogonal least-squares regression of nightly average magnitudes in B, g', r', I_C passbands against the V-band magnitude of KIC 8462852, for the window JD 2458215–300.

An approach to minimise the χ^2 of the fit to equation 4, which simultaneously confers a significant net improvement to the reduced chi-squared of the linear fits in Fig. 3, informed the rejection of a single nightly average magnitude.

3.2. *Comparison with measurements of extinction associated with the month- to year-long brightness variation*

We firmly detect a non-grey extinction for the ∼month-long variation seen across the window studied here, and the inferred $\alpha \sim 1.3$ — which translates to a preferred value of $R_V \sim 3.2$ (see below) — is suggestive of the steeper extinction also measured by Schaefer et al. (2018). This is consistent with extinction associated with dust composed of a substantial fraction of sub-micron-sized particles.

The first measurements of the extinction associated with KIC 8462852's long-term flux variations favoured a more neutral extinction (§1), with $R_V \sim 5$, implying larger grain sizes. Using an approach of χ^2 minimisation, Deeg et al. (2018) translate the R_V values of Meng et al. (2017) and Davenport et al. (2018) to $\alpha \leqslant 1.1$ and $\alpha = 1.1 \pm 0.1$ respectively. With our $\alpha = 1.33 \pm 0.43$, we cannot therefore firmly rule-out this more neutral

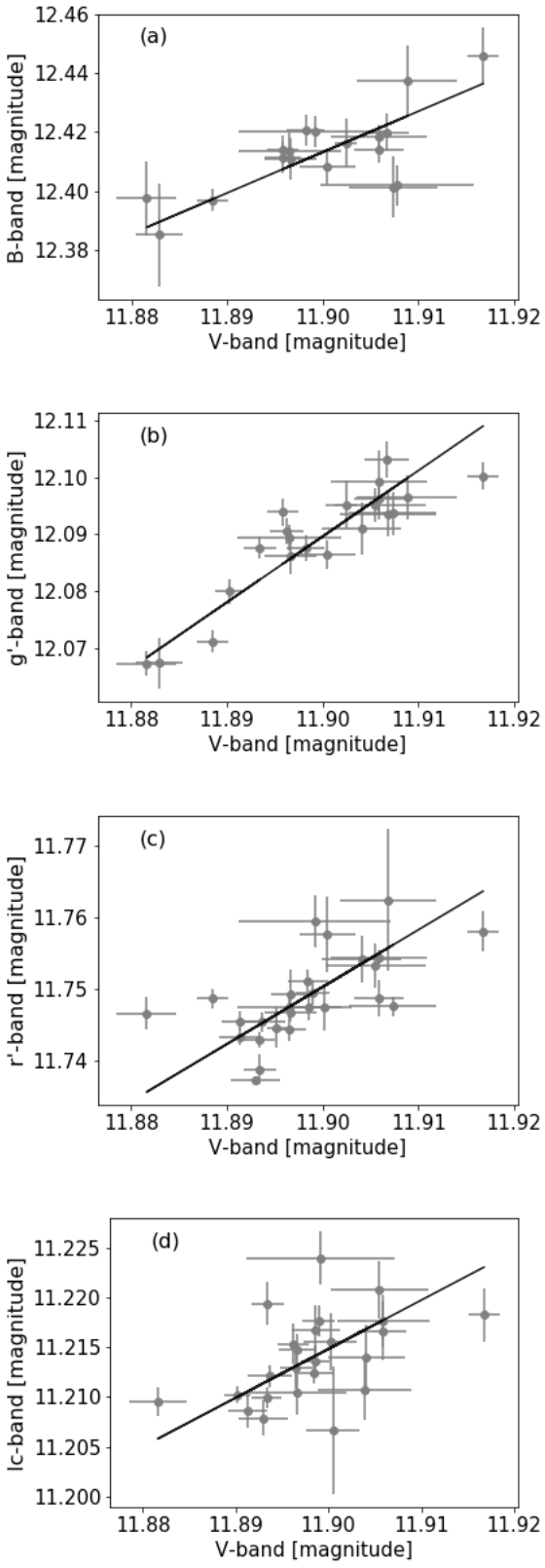

Figure 3. The nightly average magnitudes in (*a*) B, (*b*) g', (*c*) r', and (*d*) I_C passbands against the V-band magnitude of KIC 8462852, for the window JD 2458215–300; the fitted lines from a BCES orthogonal weighted least-squares fit are shown.

extinction, even at 1σ. One can also reverse the approach of Deeg et al. (2018) to convert any given α to a corresponding R_V, and for our $\alpha = 1.33 \pm 0.43$, we recover $R_V = 3.2^{+2.6}_{-1.0}$. As a check, from a weighted least-squares fitting of the values in Table 2 directly to the one-parameter extinction law of Cardelli et al. (1989), with a Monte Carlo resampling based on the uncertainties given, we infer a median $R_V = 2.9$ with lower and upper 34 percentiles of $R_V = 1.9$ and 5.5: i.e., $R_V = 2.9^{+2.6}_{-1.0}$, similar to the values obtained from our fit to α.

Despite the large range in R_V, it is interesting that our favoured value is biased towards steeper extinctions, similar to that which is associated with material in the interstellar medium. Perhaps crucially, the studies of Meng et al. (2017) and Davenport et al. (2018) relied on measurements taken hundreds of days apart, while this study, as in Schaefer et al. (2018), has used data with a time resolution of tens of days or finer. Meng et al. (2017) suffer from $\sim$ 100-day gaps in their *Swift, Spitzer* and BVR observations. The $BVRI$ light curves of Schaefer et al. (2018) reveal, however, that there is not a monotonic decline in the interval of these observations — that is, the observations have bypassed a region showing a steep rise and subsequent decline in the B and V bands of over 10 mmag in the space of $\sim$ 150 days.

3.3. *The relationship between the dips and the longer-term variation*

With the notable exception of $\alpha = 2.19 \pm 0.45$ from Deeg et al. (2018)[3], measurements of the extinction associated with dips tend towards more neutral colours than that favoured both here and by Schaefer et al. (2018) for the longer-term variation. E.g., $R_V \sim 5$ from relative depths $B/i' = 1.94 \pm 0.06$ from Boyajian et al. (2018) (see Section 6 in Schaefer et al. (2018)), and comparable $(X/i')_{dip}$ depth ratios in Bodman et al. (2018) (see Table 1 in their Section 3). The exception to this trend is *Celeste*, where Bodman et al. (2018) measure $B/i' = 3.09^{+0.18}_{-0.17}$ and $r'/i' = 1.55 \pm 0.10$, which together are suggestive of steeper extinctions, such as those favoured in this work.

There is no doubt that the dust responsible for both the day-long dips and month-to-year-long brightness variations of KIC 8462852 must be composed of a large fraction of sub-micron-sized particles. This is highly suggestive of some common origin for these phenomena,

[3] Deeg et al. (2018) do not convert their α to a corresponding R_V, but by using the approach described above it is implied to be $R_V \leqslant 2.2$, and hence, representative of a highly chromatic extinction. We note that our upper 1-σ limit for α is just consistent with their lower 1-σ limit.

which differ only in timescale. In this 'single mechanism' framework, the dips may be thought of as the substructure to the longer-term variation (Schaefer et al. 2018). Of the existing theories attempting to explain this enigmatic star's behaviour, is a contrast in extinction between the dips and longer-term variation to be expected?

The 'cometary' hypothesis, first described by Boyajian et al. (2016), postulates that the dips can be explained by the passage of a necessarily large number of objects on an highly elliptical orbit that have begun to break-up and release dust (due either to gravitational or thermal stresses) at a periastron close to our line of sight. This theory satisfies both the orbital constraints deduced from the star's light curve, in addition to the apparent absence of an infrared excess typically associated with dusty circumstellar distributions (Marengo et al. 2015; Thompson et al. 2016), since the orbital material is at almost all times far from the star, until its approach to its transit. The JD interval assessed in this work immediately follows a large dip event, and hence, in this cometary scenario, would provide a measure of extinction associated with the material composing the 'tail' of the fragmenting object(s). Wyatt et al. (2017) show how the measured chromaticity is strongly dependent on the optical depth, and indeed, one would associate a steeper extinction with the thinner trailing material than that of the dense dust distribution about the nucleus, which constitutes the cometary coma. One should also expect larger grains to be more closely bound to the nucleus, further influencing the more neutral extinction.

4. CONCLUSIONS

We present an analysis of the results of a multi-band photometric monitoring campaign of the enigmatic star, KIC 8462852, across the JD window (2450000+) 8215–8300. We measure the extinction associated with the long-term, wavelength-dependent brightness variations of the star seen over this 85-day interval of net brightening, which immediately follows a ~ 5 per cent days-long dip. We find a significant chromatic dependence in the extinction; we infer an Ångström absorption coefficient, α, of 1.33 ± 0.43 ($R_V \simeq 3.2^{+2.6}_{-1.0}$) to describe the extinction associated with this JD window, which is suggestive of a dust population composed of a substantial fraction of sub-micron-sized grains. This steep extinction is supportive of the most recent analysis of the wavelength-dependence associated with the longer-term brightness variations of the star (Schaefer et al. 2018), which together are suggestive of a typically stronger extinction than that associated with the days-long dips. That both timescales of brightness variation are associated with sub-micron sized grains suggests they may have a common origin. We cannot, however, confidently rule-out a greyer extinction ($R_V \geqslant 5$), even at 1σ, but our fitted values for α and R_V are biased towards a steep extinction, similar to that which is associated with material in the interstellar medium.

These small sub-micron sized grains would be blown out of the KIC 8462852 system on a timescale of months by the radiation pressure of the F-type star. A consequence of this — given the reality of the centuries-long Schaefer (2016) dimming — is that there must be some continually replenishing source of dust. If these reservoirs of dust are the objects associated with the dips, then further interrogation of the chromatic extinction associated with them may help clarify their nature. It will be important to continue to explore contrasts between the extinction associated with the dips and the longer-term variation through precise multi-color photometry, from which one may begin to assess the relationship between the dust and its progenitors.

We would like to extend a thank you to the supporters of the dedicated Las Cumbres Observatory Global Telescope Network (LCOGT) observing campaign aimed at this most mysterious source. The keen public interest in Tabetha Boyajian's eponymous star has allowed for high quality, short time resolution photometry, which has made possible the characterisation of the nature of this target on days-long timescales, as shown by the superimposed r'-band light curve of Boyajian et al. (2018) in Figure 2.

APPENDIX

A. THE MULTI-BAND UCLO LIGHT CURVE

Respective offsets of -0.43, -0.16, $+0.11$ and $+0.61$ are applied to the $Bg'r'I_c$ passband magnitudes in Table 3 for purposes of display in Figure 2. As in the Figure, the errors presented below are the orthogonal sum of the standard error on the nightly averages with the σ_i statistic, the derivation of which is described in Section 2.4.

Table 3. The full 1.3-year-long $Bg'Vr'I_c$ UCLO light curve for KIC 8462852.

Julian date	Passband	Magnitude	Magnitude Error
2458039.49	*B*	12.4057	0.0045
2458106.29	*B*	12.4297	0.0061
2458137.76	*B*	12.4171	0.0035
2458148.74	*B*	12.4002	0.0062
2458150.25	*B*	12.4016	0.0074
2458157.71	*B*	12.3971	0.0113
2458161.71	*B*	12.4215	0.0038
2458165.74	*B*	12.4276	0.0045
2458173.70	*B*	12.4209	0.0048
2458214.55	*B*	12.4459	0.0097
2458228.53	*B*	12.4110	0.0071
2458229.51	*B*	12.4282	0.0101
2458231.53	*B*	12.4184	0.0038
2458241.48	*B*	12.4199	0.0066
2458243.91	*B*	12.4201	0.0055
2458244.50	*B*	12.4375	0.0120
2458245.29	*B*	12.4187	0.0065
2458247.56	*B*	12.4137	0.0060
2458252.80	*B*	12.4026	0.0047
2458253.96	*B*	12.4019	0.0067
2458259.48	*B*	12.4013	0.0105
2458272.46	*B*	12.4164	0.0080
2458273.41	*B*	12.4141	0.0046
2458275.41	*B*	12.4205	0.0057
2458280.47	*B*	12.4083	0.0060
2458281.44	*B*	12.4138	0.0049
2458282.42	*B*	12.4205	0.0054
2458284.49	*B*	12.4200	0.0052
2458292.48	*B*	12.4111	0.0053
2458296.52	*B*	12.3974	0.0126
2458297.51	*B*	12.3850	0.0176
2458299.47	*B*	12.3969	0.0038
2458300.51	*B*	12.4073	0.0072
2458302.48	*B*	12.4118	0.0021
2458305.51	*B*	12.4030	0.0073
2458307.50	*B*	12.4064	0.0032
2458315.50	*B*	12.4120	0.0088
2458322.43	*B*	12.4120	0.0022
2458323.50	*B*	12.4074	0.0054
2458324.43	*B*	12.4096	0.0056
2458337.41	*B*	12.4081	0.0064
2458354.53	*B*	12.4009	0.0099
2458362.51	*B*	12.3994	0.0105
2458364.38	*B*	12.3938	0.0094
2458379.38	*B*	12.4171	0.0038
2458383.49	*B*	12.4017	0.0037
2458385.55	*B*	12.4043	0.0063
2458386.32	*B*	12.3938	0.0062

2458042.29	g'	12.0967	0.0037
2458106.30	g'	12.0897	0.0021
2458137.78	g'	12.0878	0.0030
2458148.76	g'	12.0827	0.0058
2458150.27	g'	12.0951	0.0045
2458157.73	g'	12.0956	0.0039
2458161.73	g'	12.0894	0.0025
2458165.76	g'	12.1065	0.0059
2458173.71	g'	12.0898	0.0015
2458214.57	g'	12.1002	0.0024
2458228.55	g'	12.0863	0.0033
2458229.53	g'	12.1038	0.0044
2458231.55	g'	12.0992	0.0056
2458241.50	g'	12.1032	0.0032
2458243.52	g'	12.0935	0.0038
2458244.52	g'	12.0965	0.0038
2458245.54	g'	12.0911	0.0046
2458247.58	g'	12.0895	0.0022
2458252.56	g'	12.0952	0.0030
2458254.00	g'	12.0995	0.0063
2458259.50	g'	12.0937	0.0038
2458272.48	g'	12.0952	0.0042
2458273.43	g'	12.0962	0.0036
2458275.43	g'	12.0974	0.0046
2458280.49	g'	12.0864	0.0025
2458281.46	g'	12.0939	0.0024
2458282.44	g'	12.0875	0.0023
2458292.50	g'	12.0906	0.0024
2458295.52	g'	12.0799	0.0022
2458296.54	g'	12.0673	0.0022
2458297.53	g'	12.0674	0.0045
2458298.49	g'	12.0877	0.0020
2458299.49	g'	12.0712	0.0019
2458300.52	g'	12.0830	0.0024
2458302.50	g'	12.0781	0.0029
2458305.52	g'	12.0809	0.0026
2458307.51	g'	12.0884	0.0015
2458315.52	g'	12.0889	0.0185
2458315.53	g'	12.0931	0.0063
2458322.45	g'	12.0867	0.0009
2458323.51	g'	12.0838	0.0023
2458324.45	g'	12.0852	0.0020
2458332.42	g'	12.0806	0.0030
2458337.43	g'	12.0889	0.0104
2458352.38	g'	12.0839	0.0024
2458354.55	g'	12.0780	0.0051
2458362.56	g'	12.0861	0.0049
2458364.40	g'	12.0867	0.0030
2458379.40	g'	12.0957	0.0011
2458383.51	g'	12.0913	0.0021

2458385.57	g'	12.0843	0.0028
2458386.34	g'	12.0937	0.0023
2457897.52	V	11.8999	0.0014
2457911.42	V	11.8989	0.0034
2457924.43	V	11.9116	0.0059
2457966.47	V	11.8908	0.0031
2458002.53	V	11.8957	0.0017
2458008.42	V	11.8952	0.0021
2458011.42	V	11.8865	0.0016
2458016.32	V	11.8886	0.0015
2458016.35	V	11.8808	0.0040
2458018.51	V	11.8853	0.0019
2458039.40	V	11.8752	0.0064
2458042.29	V	11.9008	0.0036
2458056.42	V	11.8825	0.0026
2458101.27	V	11.8931	0.0024
2458102.21	V	11.8949	0.0017
2458106.26	V	11.8930	0.0040
2458106.30	V	11.8970	0.0032
2458137.77	V	11.9071	0.0042
2458148.75	V	11.8948	0.0024
2458150.26	V	11.9032	0.0036
2458150.74	V	11.9055	0.0028
2458157.72	V	11.8947	0.0033
2458157.73	V	11.8989	0.0033
2458161.72	V	11.8967	0.0023
2458163.73	V	11.8955	0.0046
2458165.73	V	11.8976	0.0028
2458165.75	V	11.9048	0.0020
2458173.71	V	11.9034	0.0053
2458214.56	V	11.9168	0.0017
2458227.59	V	11.8985	0.0021
2458228.54	V	11.8966	0.0027
2458228.60	V	11.8986	0.0016
2458229.03	V	11.9016	0.0053
2458231.54	V	11.9059	0.0050
2458241.49	V	11.9067	0.0023
2458241.56	V	11.8934	0.0016
2458243.51	V	11.9068	0.0050
2458244.51	V	11.9088	0.0052
2458245.53	V	11.9041	0.0041
2458247.57	V	11.8966	0.0054
2458252.55	V	11.9055	0.0052
2458253.87	V	11.9078	0.0081
2458254.52	V	11.9002	0.0028
2458259.16	V	11.8986	0.0026
2458259.49	V	11.9073	0.0046
2458259.59	V	11.9039	0.0050
2458272.43	V	11.8967	0.0020
2458272.47	V	11.9024	0.0012

2458273.42	V	11.9058	0.0026
2458273.45	V	11.8936	0.0030
2458275.42	V	11.9091	0.0037
2458280.48	V	11.9005	0.0029
2458281.45	V	11.8958	0.0016
2458281.47	V	11.8937	0.0024
2458282.43	V	11.8982	0.0020
2458282.47	V	11.8990	0.0017
2458284.46	V	11.8992	0.0080
2458291.52	V	11.8913	0.0021
2458292.49	V	11.8959	0.0019
2458292.50	V	11.8962	0.0017
2458295.51	V	11.8914	0.0020
2458295.52	V	11.8902	0.0014
2458296.47	V	11.8965	0.0017
2458296.53	V	11.8816	0.0031
2458297.49	V	11.8930	0.0026
2458297.52	V	11.8829	0.0025
2458298.48	V	11.8934	0.0017
2458298.54	V	11.8952	0.0011
2458299.48	V	11.8885	0.0016
2458300.52	V	11.8922	0.0017
2458302.47	V	11.8953	0.0021
2458302.49	V	11.8980	0.0008
2458303.48	V	11.8961	0.0047
2458305.47	V	11.8923	0.0022
2458305.52	V	11.8899	0.0046
2458305.57	V	11.8958	0.0021
2458307.50	V	11.8962	0.0011
2458315.52	V	11.8902	0.0103
2458322.44	V	11.8914	0.0035
2458323.44	V	11.8892	0.0034
2458324.44	V	11.8897	0.0039
2458332.41	V	11.8905	0.0026
2458337.42	V	11.8853	0.0042
2458352.37	V	11.8923	0.0028
2458352.44	V	11.8907	0.0029
2458354.54	V	11.8890	0.0034
2458354.57	V	11.8860	0.0028
2458362.95	V	11.8913	0.0028
2458364.39	V	11.8980	0.0028
2458365.48	V	11.8939	0.0019
2458379.39	V	11.9058	0.0023
2458383.50	V	11.8930	0.0029
2458385.56	V	11.8901	0.0036
2458386.33	V	11.8924	0.0044
2457897.51	r'	11.7510	0.0011
2457911.42	r'	11.7530	0.0027
2457924.43	r'	11.7626	0.0024
2457947.43	r'	11.7500	0.0036

2457955.41	r'	11.7541	0.0024
2457955.52	r'	11.7580	0.0017
2457966.43	r'	11.7486	0.0015
2457966.52	r'	11.7490	0.0014
2458002.51	r'	11.7536	0.0021
2458008.40	r'	11.7514	0.0034
2458011.40	r'	11.7465	0.0015
2458016.31	r'	11.7419	0.0036
2458018.49	r'	11.7407	0.0014
2458106.28	r'	11.7379	0.0044
2458137.74	r'	11.7527	0.0036
2458137.76	r'	11.7428	0.0029
2458148.76	r'	11.7382	0.0055
2458150.75	r'	11.7567	0.0029
2458150.75	r'	11.7460	0.0028
2458157.72	r'	11.7519	0.0031
2458157.74	r'	11.7490	0.0022
2458159.76	r'	11.7419	0.0039
2458161.74	r'	11.7537	0.0066
2458163.74	r'	11.7442	0.0026
2458165.72	r'	11.7602	0.0026
2458165.74	r'	11.7447	0.0014
2458173.73	r'	11.7492	0.0013
2458174.71	r'	11.7489	0.0021
2458214.59	r'	11.7581	0.0028
2458227.58	r'	11.7512	0.0015
2458228.57	r'	11.7468	0.0012
2458228.59	r'	11.7475	0.0019
2458231.57	r'	11.7543	0.0011
2458241.55	r'	11.7430	0.0011
2458241.58	r'	11.7496	0.0022
2458243.48	r'	11.7625	0.0098
2458245.48	r'	11.7542	0.0033
2458247.59	r'	11.7475	0.0015
2458252.48	r'	11.7533	0.0032
2458254.01	r'	11.7502	0.0025
2458254.50	r'	11.7474	0.0033
2458257.52	r'	11.7452	0.0020
2458257.52	r'	11.7441	0.0022
2458259.45	r'	11.7488	0.0031
2458259.50	r'	11.7476	0.0014
2458272.43	r'	11.7494	0.0034
2458273.42	r'	11.7488	0.0026
2458273.53	r'	11.7440	0.0018
2458275.52	r'	11.7466	0.0014
2458275.54	r'	11.7447	0.0012
2458280.49	r'	11.7576	0.0052
2458281.47	r'	11.7454	0.0013
2458281.53	r'	11.7501	0.0020
2458282.46	r'	11.7495	0.0016

2458282.49	r'	11.7489	0.0012
2458284.45	r'	11.7595	0.0036
2458284.46	r'	11.7484	0.0014
2458291.51	r'	11.7433	0.0011
2458295.52	r'	11.7456	0.0013
2458295.54	r'	11.7472	0.0008
2458296.48	r'	11.7444	0.0017
2458296.48	r'	11.7466	0.0022
2458297.48	r'	11.7373	0.0005
2458298.50	r'	11.7388	0.0021
2458298.51	r'	11.7446	0.0028
2458299.50	r'	11.7487	0.0014
2458300.47	r'	11.7449	0.0018
2458302.53	r'	11.7420	0.0016
2458302.57	r'	11.7359	0.0035
2458303.54	r'	11.7424	0.0024
2458303.59	r'	11.7459	0.0027
2458305.52	r'	11.7466	0.0017
2458307.52	r'	11.7433	0.0014
2458310.51	r'	11.7390	0.0028
2458315.54	r'	11.7353	0.0028
2458323.40	r'	11.7501	0.0021
2458324.40	r'	11.7346	0.0025
2458331.54	r'	11.7268	0.0019
2458337.44	r'	11.7450	0.0043
2458352.44	r'	11.7453	0.0013
2458352.50	r'	11.7326	0.0025
2458354.56	r'	11.7409	0.0038
2458354.62	r'	11.7236	0.0029
2458362.57	r'	11.7252	0.0039
2458363.38	r'	11.7405	0.0011
2458364.48	r'	11.7284	0.0033
2458365.47	r'	11.7457	0.0010
2458383.52	r'	11.7097	0.0024
2458386.44	r'	11.7377	0.0024
2457897.54	I_c	11.2144	0.0022
2457911.44	I_c	11.2066	0.0040
2457924.45	I_c	11.2240	0.0022
2457947.43	I_c	11.2234	0.0032
2457955.53	I_c	11.2202	0.0015
2457966.52	I_c	11.2074	0.0019
2458002.52	I_c	11.2128	0.0014
2458008.41	I_c	11.2167	0.0012
2458011.41	I_c	11.2107	0.0024
2458016.32	I_c	11.2060	0.0022
2458018.50	I_c	11.2093	0.0014
2458039.41	I_c	11.2106	0.0016
2458054.44	I_c	11.2142	0.0040
2458056.44	I_c	11.1952	0.0016
2458066.33	I_c	11.1901	0.0056

2458101.29	I_c	11.1862	0.0052
2458102.23	I_c	11.2079	0.0015
2458106.28	I_c	11.2022	0.0032
2458106.28	I_c	11.2218	0.0029
2458116.33	I_c	11.2214	0.0026
2458137.75	I_c	11.2149	0.0028
2458148.76	I_c	11.1992	0.0032
2458150.75	I_c	11.2243	0.0048
2458150.76	I_c	11.2113	0.0017
2458157.71	I_c	11.2119	0.0062
2458157.75	I_c	11.2087	0.0021
2458163.75	I_c	11.1971	0.0066
2458165.73	I_c	11.2347	0.0057
2458165.75	I_c	11.2111	0.0013
2458173.74	I_c	11.2079	0.0033
2458174.71	I_c	11.2265	0.0023
2458214.62	I_c	11.2182	0.0027
2458227.59	I_c	11.2125	0.0012
2458228.60	I_c	11.2136	0.0015
2458228.60	I_c	11.2044	0.0035
2458229.54	I_c	11.2222	0.0054
2458231.58	I_c	11.2177	0.0026
2458241.56	I_c	11.2099	0.0010
2458241.58	I_c	11.2171	0.0013
2458245.49	I_c	11.2140	0.0033
2458247.60	I_c	11.2105	0.0023
2458252.50	I_c	11.2208	0.0029
2458253.68	I_c	11.2188	0.0025
2458254.51	I_c	11.2212	0.0031
2458254.51	I_c	11.2156	0.0029
2458258.92	I_c	11.2123	0.0013
2458259.17	I_c	11.2167	0.0024
2458259.59	I_c	11.2107	0.0031
2458272.44	I_c	11.2147	0.0016
2458273.43	I_c	11.2166	0.0029
2458275.54	I_c	11.2196	0.0024
2458275.55	I_c	11.2179	0.0019
2458280.50	I_c	11.2066	0.0064
2458281.47	I_c	11.2121	0.0011
2458281.54	I_c	11.2111	0.0013
2458282.47	I_c	11.2176	0.0016
2458282.50	I_c	11.2122	0.0014
2458284.46	I_c	11.2239	0.0027
2458291.52	I_c	11.2086	0.0017
2458292.51	I_c	11.2153	0.0020
2458295.52	I_c	11.2102	0.0008
2458295.55	I_c	11.2042	0.0047
2458296.49	I_c	11.2129	0.0020
2458296.49	I_c	11.2095	0.0014
2458297.48	I_c	11.2072	0.0035

2458297.49	I_c	11.2079	0.0018
2458298.43	I_c	11.2104	0.0015
2458298.51	I_c	11.2194	0.0021
2458298.57	I_c	11.2154	0.0018
2458300.48	I_c	11.2102	0.0016
2458302.49	I_c	11.2099	0.0008
2458302.51	I_c	11.2065	0.0027
2458302.58	I_c	11.2051	0.0036
2458303.55	I_c	11.2055	0.0015
2458303.60	I_c	11.1996	0.0030
2458305.48	I_c	11.2090	0.0014
2458305.54	I_c	11.2109	0.0008
2458305.57	I_c	11.2105	0.0015
2458307.53	I_c	11.2096	0.0016
2458310.52	I_c	11.2022	0.0023
2458315.55	I_c	11.2131	0.0010
2458322.53	I_c	11.2131	0.0008
2458324.41	I_c	11.2201	0.0042
2458331.44	I_c	11.2124	0.0016
2458337.43	I_c	11.2090	0.0043
2458352.44	I_c	11.2082	0.0016
2458354.57	I_c	11.2026	0.0019
2458354.64	I_c	11.2015	0.0037
2458362.58	I_c	11.2013	0.0034
2458363.40	I_c	11.2118	0.0016
2458364.50	I_c	11.2059	0.0032
2458365.50	I_c	11.2129	0.0015
2458386.43	I_c	11.2142	0.0021

REFERENCES

Akritas, M. G., & Bershady, M. A. 1996, arXiv preprint astro-ph/9605002

Bertin, E., & Arnouts, S. 1996, Astronomy and Astrophysics Supplement Series, 117, 393

Bodman, E., Wright, J., Boyajian, T., & Ellis, T. 2018, arXiv preprint arXiv:1806.08842

Boyajian, T., LaCourse, D., Rappaport, S., et al. 2016, Monthly Notices of the Royal Astronomical Society, 457, 3988

Boyajian, T. S., Alonso, R., Ammerman, A., et al. 2018, The Astrophysical Journal Letters, 853, L8

Cardelli, J. A., Clayton, G. C., & Mathis, J. S. 1989, The Astrophysical Journal, 345, 245

Davenport, J. R., Covey, K. R., Clarke, R. W., et al. 2018, The Astrophysical Journal, 853, 130

Deeg, H. J., Alonso, R., Nespral, D., & Boyajian, T. S. 2018, Astronomy & Astrophysics, 610, L12

Henden, A., Templeton, M., Terrell, D., et al. 2016, VizieR Online Data Catalog, 2336

Lahey, A., Dimick, D., & Layden, A. 2017, Journal of the American Association of Variable Star Observers (JAAVSO), 45, 202

Marengo, M., Hulsebus, A., & Willis, S. 2015, The Astrophysical Journal Letters, 814, L15

Meng, H. Y., Rieke, G., Dubois, F., et al. 2017, The Astrophysical Journal, 847, 131

Moosmüller, H., Chakrabarty, R., Ehlers, K., & Arnott, W. 2011, Atmospheric Chemistry and Physics, 11, 1217

Osborn, H. P., Kenworthy, M., Rodriguez, J. E., et al. 2019, Monthly Notices of the Royal Astronomical Society

Schaefer, B. E. 2016, The Astrophysical Journal Letters, 822, L34

Schaefer, B. E., Bentley, R. O., Boyajian, T. S., et al. 2018, Monthly Notices of the Royal Astronomical Society, 481, 2235

Thompson, M., Scicluna, P., Kemper, F., et al. 2016, Monthly Notices of the Royal Astronomical Society: Letters, 458, L39

Wyatt, M. C., van Lieshout, R., Kennedy, G. M., & Boyajian, T. 2017, Monthly Notices of the Royal Astronomical Society, 473, 5286